Acta Biomaterialia 104 (2020) 53–65

Contents lists available at ScienceDirect

Acta Biomaterialia

journal homepage: www.elsevier.com/locate/actbio

Full length article

Towards microstructure-informed material models for human brain tissue

S. Budday[a,*], M. Sarem[b,c], L. Starck[b,c], G. Sommer[d], J. Pfefferle[a], N. Phunchago[e], E. Kuhl[f], F. Paulsen[e,i], P. Steinmann[a,g], V.P. Shastri[b,c,*], G.A. Holzapfel[d,h,*]

[a] Department of Mechanical Engineering, Friedrich-Alexander-University Erlangen-Nürnberg (FAU), Erlangen 91058, Germany
[b] Institute for Macromolecular Chemistry, University of Freiburg, Freiburg 79104, Germany
[c] BIOSS Centre for Biological Signalling Studies, University of Freiburg, Freiburg 79104, Germany
[d] Institute of Biomechanics, Graz University of Technology, Graz 8010, Austria
[e] Institute of Anatomy, Friedrich-Alexander-University Erlangen-Nürnberg (FAU), Erlangen 91058, Germany
[f] Departments of Mechanical Engineering & Bioengineering, Stanford University, CA 94305, USA
[g] Glasgow Computational Engineering Centre, University of Glasgow, Glasgow, UK
[h] Faculty of Engineering Science and Technology, Norwegian University of Science and Technology (NTNU), Trondheim 7491, Norway
[i] Department of Topographic Anatomy and Operative Surgery, Sechenov University, Moscow, Russia

ARTICLE INFO

Article history:
Received 13 August 2019
Revised 19 December 2019
Accepted 20 December 2019
Available online 27 December 2019

Keywords:
Material modeling
Biomechanical testing
Hyperelasticity
Ogden model
Human brain tissue
Microstructure

ABSTRACT

Emerging evidence suggests that the mechanical behavior of the brain plays a critical role in development, disease, and aging. Recent studies have begun to characterize the mechanical behavior of gray and white matter tissue and to identify sets of material models that best reproduce the stress-strain behavior of different brain regions. Yet, these models are mainly phenomenological in nature, their parameters often lack clear physical interpretation, and they fail to correlate the mechanical behavior to the underlying microstructural composition. Here we make a first attempt towards identifying general relations between microstructure and mechanics with the ultimate goal to develop microstructurally motivated constitutive equations for human brain tissue. Using histological staining, we analyze the microstructure of brain specimens from different anatomical regions, the cortex, basal ganglia, corona radiata, and corpus callosum, and identify the regional stiffness and viscosity under multiple loading conditions, simple shear, compression, and tension. Strikingly, our study reveals a negative correlation between cell count and stiffness, a positive correlation between myelin content and stiffness, and a negative correlation between proteoglycan content and stiffness. Additionally, our analysis shows a positive correlation between lipid and proteoglycan content and viscosity. We demonstrate how understanding the microstructural origin of the macroscopic behavior of the brain can help us design microstructure-informed material models for human brain tissue that inherently capture regional heterogeneities. This study represents an important step towards using brain tissue stiffness and viscosity as early diagnostic markers for clinical conditions including chronic traumatic encephalopathy, Alzheimer's and Parkinson's disease, or multiple sclerosis.

Statement of significance

The complex and heterogeneous mechanical properties of brain tissue play a critical role for brain function. To understand and predict how brain tissue properties vary in space and time, it will be key to link the mechanical behavior to the underlying microstructural composition. Here we use histological staining to quantify area fractions of microstructural components of mechanically tested specimens and evaluate their individual contributions to the nonlinear macroscopic mechanical response. We further propose a microstructure-informed material model for human brain tissue that inherently captures regional heterogeneities. The current work provides unprecedented insights into the biomechanics of human brain tissue, which are highly relevant to develop refined computational models for brain tissue behavior or to advance neural tissue engineering.

* Corresponding authors.
E-mail addresses: silvia.budday@fau.de (S. Budday), prasad.shastri@gmail.com (V.P. Shastri), holzapfel@tugraz.at (G.A. Holzapfel).

https://doi.org/10.1016/j.actbio.2019.12.030
1742-7061/

1. Introduction

Over the past several decades, cumulative evidence has emerged that mechanics plays a critical role in neurological disorders [1,2], including – among many others – stroke, dementia, and epilepsy, which are major threats to public health according to the world health organization. External impacts to the brain can cause damage to brain tissue during traumatic brain injury [3,4], but, on a much smaller scale, mechanical cues also influence cell behavior and function [2,5,6]. Therefore, understanding to what extent the microstructural components affect the macroscopic mechanical behavior is key to gain further insights into the mechanisms of injury and disease in the human brain. Vice versa, recent studies have shown that an increase in the extracellular matrix stiffness can enhance tumor cell migration, proliferation, and invasion [7]. More recently, it has been demonstrated that neurons and astrocytes perceive and process nanoscale topography such as those associated with glycosaminoglycans (GAGs) as localized mechanical perturbations through mechanosensing stretch-activated protein channels such as Piezo-1 [8]. Importantly, for many pathological conditions, such as degenerative diseases, microstructural changes have been investigated; however, the link between changes in the microstructural components and the corresponding tissue mechanics or macrostructural tissue properties remains to be clarified [9]. Addressing this issue could enhance the potential of early in vivo diagnostics using modern imaging techniques in combination with numerical simulations based on continuum mechanical modeling. Mechanical models can further assist in the development of novel treatment strategies or the detailed planning of surgical procedures [10].

Unlike many other soft tissues, brain tissue lacks key fibrillar extracellular matrix components such as elastin and fibrillar collagen, which control the overall mechanical behavior [12]. Interestingly, the cells in the central nervous system are also very soft compared to cells in other tissues [13]. This contributes to the low elastic modulus and the high compliance of brain tissue [2]. Another challenge in understanding the link between microstructure and mechanics of brain tissue is the exceptional heterogeneity resulting from differences in the local functional demands within our brain. While we can clearly distinguish two tissue types on the macroscopic scale, gray and white matter (see Fig. 1a), the tissue's microstructure varies significantly even within those regions. On the one hand, the composition of different cell types such as neurons, astrocytes, oligodendrocytes, or microglia, and even their morphology changes locally; on the other hand, extracellular matrix components such as proteoglycans, hyaluronic acid, and non-fibrillar collagens may again show different regional distributions than cells.

Previous studies relating microstructural components to macrostructural properties indicate that tissue stiffness increases with myelination during development in white matter [14,15], and that stiffness negatively correlates with a structural parameter called fractional anisotropy, which can be determined from magnetic resonance imaging and diffusion tensor imaging [11]. However, a systematic study of both the mechanical properties on the continuum scale and the underlying microstructure – considering both cellular and extracellular matrix components – is still missing. It remains unclear which microstructural constituents control the complex mechanical properties of brain tissue, where elastic, viscous or porous properties show distinct regional trends [16,17].

To tackle this question, in the current work, we simultaneously analyze the microstructure and mechanics of human brain tissue specimens from different anatomical regions, the cortex (C), the outer gray matter layer containing the neuronal cell bodies as the processing units of our brain, the basal ganglia (BG), inner gray matter, the corpus callosum (CC), white matter with high fiber density, mostly consisting of uniaxially oriented nerve fiber bundles (commissural fibers) running between the two hemispheres, and the corona radiata (CR), (the outer) white matter with lower fiber density. We evaluate the individual contributions of cellular and extracellular constituents to the macroscopic mechanical response under physiological conditions, with special focus on nonlinear and time-dependent effects, and present a microstructure-informed material model that can predict the spatial heterogeneity of brain tissue behavior.

2. Materials and methods

In order to gain more insights into the correlation between microstructural components and macroscopic properties of human brain tissue, this study combines the assessment of cellular and extracellular components through histological staining with the mechanical characterization through biomechanical testing. Brain samples were obtained from a 55 year old female and 68 year old male donor who were determined not to suffer from neurological diseases. For more details, we refer to [11]. Fig. 1a shows an exemplary tissue slice, where we extracted specimens from four

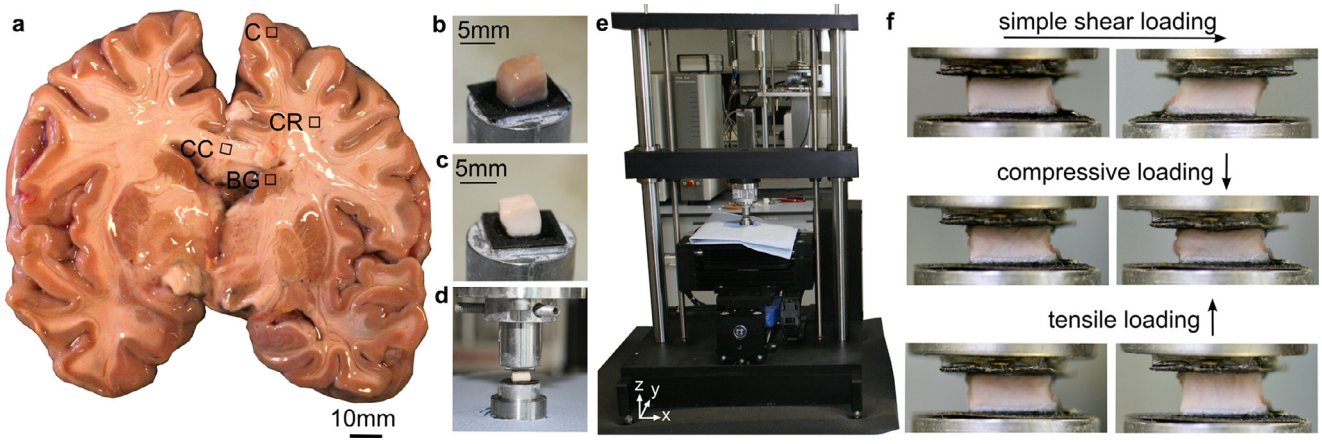

Fig. 1. Biomechanical testing setup. a) Exemplary human brain tissue slice, where the locations of specimen extraction are marked with black rectangles, adapted from [11]. Specimens were taken from four different brain regions, the corpus callosum (CC), the corona radiata (CR), the basal ganglia (BG), and the cortex (C). b) Gray matter specimen mounted to the upper specimen holder. c) White matter specimen mounted to the upper specimen holder. d) White matter specimen mounted to the testing device. e) Triaxial biomechanical testing device. f) Close ups of the tissue deformation during simple shear, compressive, and tensile loadings.

microstructurally differing brain regions, the cortex, the basal ganglia, the corpus callosum, and the corona radiata. In the current work, we present data from one specimen of each of those regions from each of the two brains. We specifically chose specimens for the microstructural investigation that had shown a mechanical response close to the average response over all specimens from a total of 10 brains tested in [11].

2.1. Mechanical characterization

In order to quantify the mechanical properties of human brain tissue, we performed biomechanical tests under multiple loading modes, simple shear, compression, and tension, as illustrated in Fig. 1f [11]. We tested all samples between 24 and 60 h *post mortem*. To minimize tissue degradation, we kept the tissue refrigerated at 3°C and humidified with phosphate-buffered saline solution at all times. We analyzed one specimen measuring approximately 5 × 5 × 5 mm from each of the four different regions of interest, the corpus callosum (CC), the corona radiata (CR), the basal ganglia (BG), and the cortex (C) (see Fig. 1a–c) [11]. We mounted each specimen onto the triaxial testing device, as shown in Fig. 1d and e, to perform simple shear, compression and tension loadings at a speed of $v = 2$ mm/min. We conducted all tests at room temperature [11].

The testing protocol started with sinusoidal simple shear up to an amount of shear of $\gamma = 0.2$ with a speed of $v = 2$ mm/min and a strain rate of approximately 0.0067 1/s in the x- and y-directions, where the amount of shear γ specifies the relative in-plane displacement of two parallel layers in the material body divided by their separation distance. The lower platform moves relative to the fixed upper platform using a biaxial translation stage up to a maximum displacement $\Delta x = \Delta y = 0.2H$ depending on specimen height H. We calculated the shear stresses $\tau_{xz/yz} = f/A$ as the force f recorded in the direction of shear divided by the shear area $A = WL$ with the specimen length L and the specimen width W. Upon completion of each direction, we also conducted stress relaxation tests to probe the viscoelastic properties of the tissue. We applied a rapid shear step up to $\gamma = 0.2$ with a speed of $v = 100$ mm/min and a strain rate of approximately 0.33 1/s, and recorded the resulting forces for a period of 300 s.

Subsequently, we similarly conducted an unconfined uniaxial compression test up to 10% compressive strain, a stress relaxation test of 300 s holding at 10% compression, and a uniaxial extension test up to 10% tensile strain. Herefore, the upper platform moved in the z-direction and we computed the stretch $\lambda = 1 + \Delta z/H$ with the specimen height H and the z-displacement Δz. As a measure of tissue stress, we determined the Piola stress P_{zz} as the force f_z in z-direction divided by the cross-sectional area A of the specimen in the unloaded configuration, i.e. $P_{zz} = f_z/A$. We recorded the forces in the three orthogonal directions (x, y, z) [18]. For each loading mode, we conducted two pre-conditioning cycles and one main cycle, which was used for further data analysis.

For each tested cube, we determined the initial shear modulus μ as a measure of tissue stiffness, and the material nonlinearity parameter α, by calibrating the modified one-term Ogden strain-energy function

$$\psi = 2\mu/\alpha^2[\lambda_1^\alpha + \lambda_2^\alpha + \lambda_3^\alpha - 3] \tag{1}$$

with the response of all conducted loading modes simultaneously [11,19]. Substituting the principal stretches for compression/tension, $\lambda_{1,c} = \lambda_{2,c} = 1/\sqrt{\lambda}$ and $\lambda_{3,c} = \lambda$, or shear, $\lambda_{1/2,s} = \gamma/2 \pm \sqrt{1 + \gamma^2/4}$ and $\lambda_{3,s} = 1$, we calculated the model predictions for the Piola stresses by deriving the strain energy with respect to the deformation, $P_{zz}^\Psi = \partial\Psi/\partial\lambda$ and $P_{xz/yz}^\Psi = \partial\Psi/\partial\gamma$. We then determined the parameters μ and α, which best represent the experimental data, by minimizing the objective function $\chi^2 = \sum_{i=1}^{n_s}(P_{xz} - P_{xz}^\Psi)_i^2 + \sum_{i=1}^{n_c+n_t}(P_{zz} - P_{zz}^\Psi)_i^2$, where n_s, n_c, and n_t are the number of considered experimental data points for shear, compression, and tension loadings, with the nonlinear least-squares algorithm *lsqnonlin* in MATLAB Release 2018b.

To evaluate the stress relaxation behavior, we determined the stress relaxation after 5 min during compression. In addition, we quantified the relaxation response by adopting a two-term Prony series,

$$\sigma(t) = \sigma_\infty + \sum_{i=1}^{2}[\sigma_i - \sigma_\infty]\exp(-t/\tau_i), \tag{2}$$

with two characteristic time constants τ_i [20]. Several previous studies had shown that two time scales are required to capture the time-dependent characteristics of brain tissue [20–23].

2.2. Microstructural analysis

2.2.1. Histological staining

Following biomechanical testing, we fixed each specimen using 4% Formaldehyde. We washed one representative specimen from each region with PBS, soaked it in 30% sucrose overnight at 4 °C in the refrigerator, embedded it in optimal cutting temperature compound, and cryosectioned 6 µm thick slices. We then used five different stains to examine cellular and extracellular constituents of the tested samples, as shown in Figs. 2, 8, and 9.

To visualize cellular elements of human brain tissue, we used Hematoxylin & Eosin (AppliChem, Germany), Klüver-Barrera, and Nissl staining: Klüver–Barrera stains myelin wrapped around nerve fibers in blue, neuropil in pink, and cells bodies in purple; the Nissl stain stains neuropil in a granular purple-blue. To visualize extracellular elements, we stained sections with Alcian Blue (Sigma-Aldrich, Germany) to visualize GAG production. In addition, we visualized the total collagen content and neutral triglycerides, as well as lipids, using Massons's Trichrome staining (Anilin blue variation, RAL DIAGNOSTICS, Martillac, France) and Oil Red staining, respectively [24,25]. While staining for cellular components was performed on specimens from both brains, the extracellular matrix components were only analyzed for the male brain, which was the brain we had tested most recently. We took images at various magnifications using a microscope, Keyence BZ-9000.

2.2.2. Image analysis

Using the image analysis tools of MATLAB Release 2018b, we quantified the relative area fraction of the red- and blue-colored regions for the different stains introduced in Section 2.2.1. The algorithm counts the pixels that are above or below a color- and stain-specific threshold. We interpreted the amount of blue in Klüver-Barrera stained images as myelin content [14], the amount of red in Oil Red stained images as lipid content, the amount of blue in Alcian Blue stained images as proteoglycan content, the amount of red in Masson's Thrichrome stained images as cytoplasm content, and the amount of blue in Masson's thrichome stained images as collagen content [26]. Fig. 3 shows an exemplary evaluation of a Masson's trichrome stained image at 10x magnification. We further determined the density of cell nuclei from Klüver–Barrera and Nissl stained images by using the cell counting algorithm presented in [27]. We performed a sensitivity analysis towards the magnification used for image analysis. While the absolute values of area fractions showed certain variations when evaluating the images at different magnifications, the regional trends were surprisingly consistent. To determine the relative area fractions of myelin, lipids, proteoglycans, collagen, and cytoplasm, we evaluated images at 10x magnification; to determine the density of cell nuclei, we used 20x magnification.

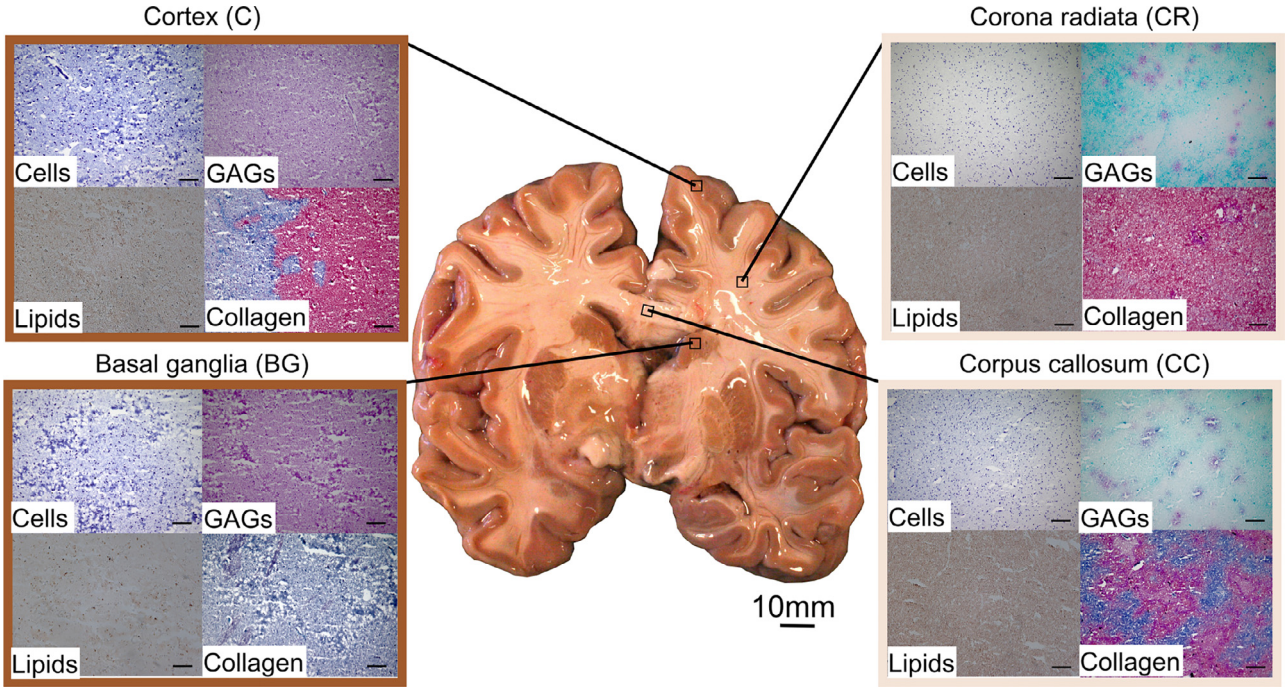

Fig. 2. Microstructure of human brain tissue. Nissl staining was used to quantify the density of cell nuclei, Alcian Blue staining to visualize the proteoglycan content, Oil Red staining to visualize lipids in brain tissue, and Masson's Trichrome staining to visualize the collagen and cytoplasm content. Images are shown at 10x magnification. Scale bars indicate 100 µm.

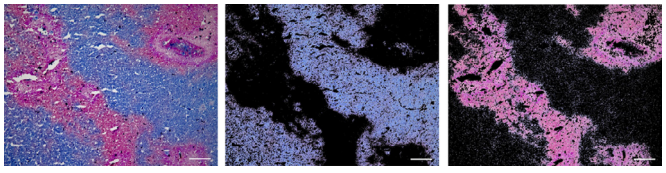

Fig. 3. Exemplary analysis of a Masson's Trichrome stained image at 10x magnification (left), where the amount of blue represents the collagen content (center), and the amount of red represents the cytoplasm content (right). Images are shown at 10x magnification. Scale bars indicate 100 µm. (For interpretation of the references to color in this figure legend, the reader is referred to the web version of this article.)

2.3. Statistical analysis

To evaluate significant differences in the microstructural composition and mechanical properties of different brain regions, we performed statistical analyses with the Statistics Toolbox in MATLAB Release 2018b. We performed a one-way analysis of variance (ANOVA) followed by a Tukey–Kramer (T–K) test for multiple comparisons for each stain to identify significant dependencies between different regions (CC, CR, BG, and C). We consider a p-value lower than 0.05 to be significant. To graphically include the results in the boxplots in Figs. 8 and 9, we denote statistically different groups by different letters (a–d). If a certain region showed no significant difference to any other region, no letter is put above the box.

3. Results

3.1. Mechanics of human brain tissue

Fig. 4 illustrates the mechanical response of brain tissue from different brain regions, the cortex, the basal ganglia, the corona radiata, and the corpus callosum. The qualitative behavior is similar for all regions: it is characterized by a pronounced hysteresis for cyclic loading, nonlinearity, and higher stresses in compression than in tension. To quantify the highly nonlinear, time-dependent mechanical response of brain tissue, we evaluate the experimental curves based on the theory of nonlinear continuum mechanics.

3.1.1. Time-independent properties

Fig. 5a shows the time-independent, hyperelastic response of human brain tissue, which we obtained by averaging between the loading and unloading segment in Fig. 4 [11]. To quantify this highly nonlinear tissue response, we used the modified one-term Ogden model as described in Section 2.1. This model has previously been shown to best represent the time-independent response of brain tissue [11,28]. The corresponding shear moduli μ and nonlinearity parameters α are shown in Fig. 5b and c. The initial shear modulus is highest for the sample from the cortex, while the nonlinearity is highest in the corona radiata and lowest in the basal ganglia.

3.1.2. Time-dependent properties

Fig. 6 summarizes the time-dependent characteristics in different brain regions. Fig. 6a shows the stress relaxation behavior in compression. As shown in Fig. 6b, the stress relaxation after 5 minutes is generally higher in white matter regions than in gray matter regions, which indicates a difference in the viscous properties of those tissue types.

Fig. 6c and d show the short and long time scales τ_1 and τ_2. Independent of the brain region, the second time constant is almost two orders of magnitude higher than the first one. According to our previous results, the first time constant could be associated with viscoelastic effects of cells, while the second time constant represents the movement of cerebrospinal fluid within the solid skeleton of cells and extracellular matrix [16,17]. The first time constant is highest in the corona radiata and lowest in the cortex, which suggests that the cellular network in the corona radiata has a higher viscosity than the one in the cortex. The second time constant is lower in both gray matter regions than in both white

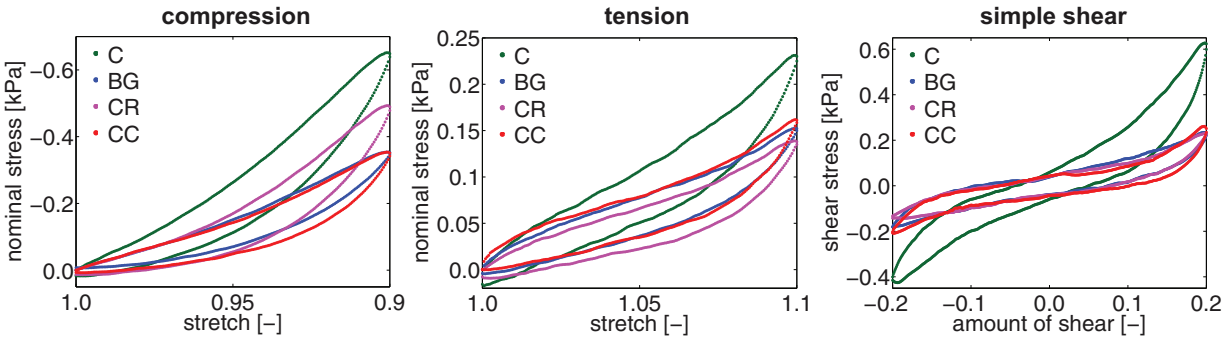

Fig. 4. Response of human brain tissue from different regions, cortex (C), basal ganglia (BG), corona radiata (CR), and corpus callosum (CC) under compression, tension, and simple shear loading.

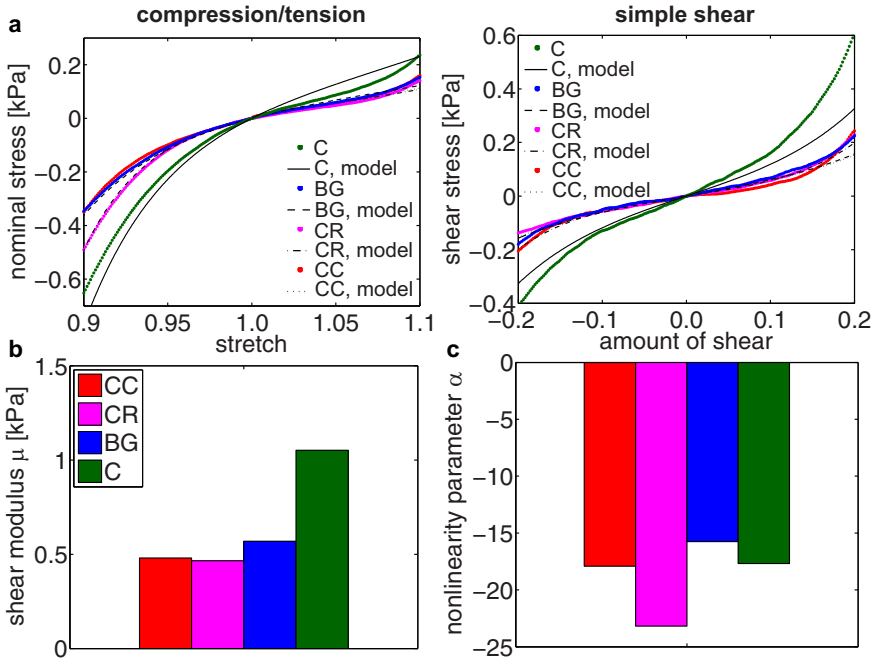

Fig. 5. Time-independent properties of human brain tissue. a) Hyperelastic response of an exemplary specimen from four different brain regions, the cortex (C), the basal ganglia (BG), the corona radiata (CR), and the corpus callosum (CC) during compression, tension, and simple shear loadings with corresponding model fit (see Eq. (1)). The mechanical response is nonlinear, compression-tension-asymmetric, and region-dependent. b) Shear moduli μ for different brain regions. c) Nonlinearity parameters α in different brain regions.

matter regions, which indicates that the permeability in white matter is lower than in gray matter.

3.2. Microstructure of human brain tissue

Fig. 2 illustrates the composition of the brain's microstructure in different anatomical regions, the cortex, the basal ganglia, the corona radiata, and the corpus callosum, visualized using histological staining. A schematic illustration of the relevant cellular and extracellular components in the human brain is shown in Fig. 7. This schematic figure is for illustration purpose only and not drawn to scale. Regarding cellular components, gray matter contains neuronal cell bodies, protoplasmic astrocytes, and microglia. White matter contains oligodendrocytes, which wrap myelin sheath around the axons, fibrous astrocytes, and microglia. The extracellular matrix in the central nervous system has, in general, three principal compartments: the basement membrane (basal lamina), which lines cerebral microvessels (and the pial surface) and connects endothelial cells to astrocytic endfeet [29], the neural interstitial matrix, which is diffusely distributed in the brain's interstitial space, and perineuronal nets, which surround inhibitory interneurons in certain areas of gray matter [7]. In different compositions, these compartments contain proteoglycans, hyaluronic acid, link proteins, glycoproteins (e.g., tenascin, laminin, fibronectin), and non-fibrillar collagens type IV and VI [7,29]. In the following, we discuss the region-specific distribution of certain constituents introduced in Section 2.2.1 and visualized in Fig. 2. Table 1 summarizes the corresponding p-values obtained from T–K tests to evaluate the statistical significance of regional differences.

Table 1
Tukey-Kramer test p-values from multiple comparisons between different brain regions, corpus callosum (CC), corona radiata (CR), basal ganglia (BG), and cortex (C), for different microstructural components, cells, myelin, lipids, proteoglycans, collagen, and cytoplasm.

p-value	Cells	Myelin	Lipids	Proteoglycans	Collagen	Cytoplasm
CC-CR	0.19	0.95	0.66	0.85	0.0001	0.01
CC-BG	0.0001	0.0001	0.08	0.0001	0.39	0.0001
CC-C	0.0001	0.0001	0.30	0.0001	0.72	0.01
CR-BG	0.0001	0.0001	0.01	0.0001	0.0001	0.0001
CR-C	0.0001	0.0001	0.04	0.0001	0.01	0.0001
BG-C	0.84	0.99	0.87	1.00	0.04	0.01

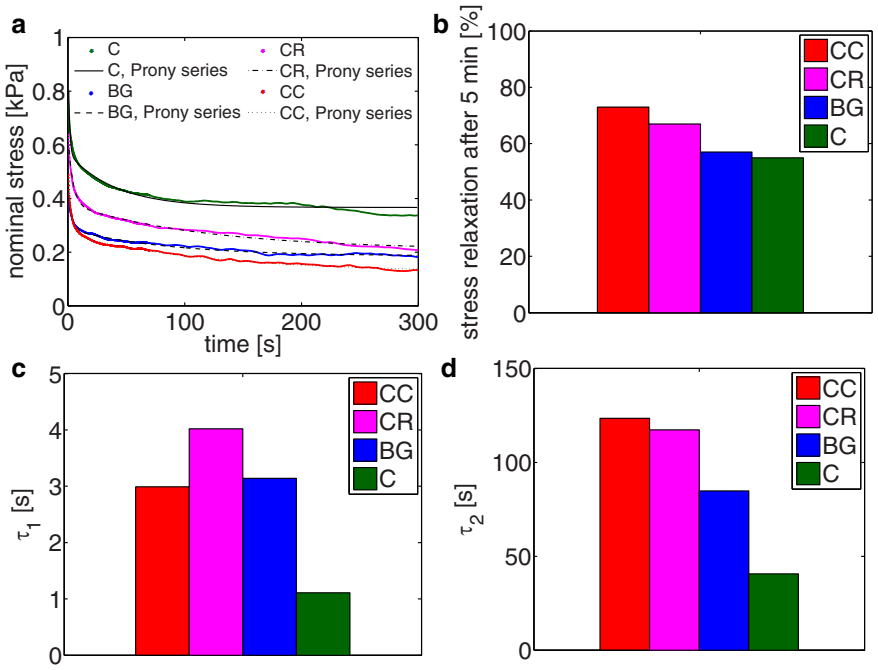

Fig. 6. Time-dependent properties of human brain tissue. a) Stress relaxation behavior of an exemplary specimen from four different brain regions, the cortex (C), the basal ganglia (BG), the corona radiata (CR), and the corpus callosum (CC) under compression loading with corresponding Prony series fit (see Eq. (2)). b) Stress relaxation after 5min for different brain regions. White matter (CR and CC) relaxes faster than gray matter (C and BG). c) Smaller time constant τ_1 for different brain regions. d) Larger time constant τ_2 for different brain regions.

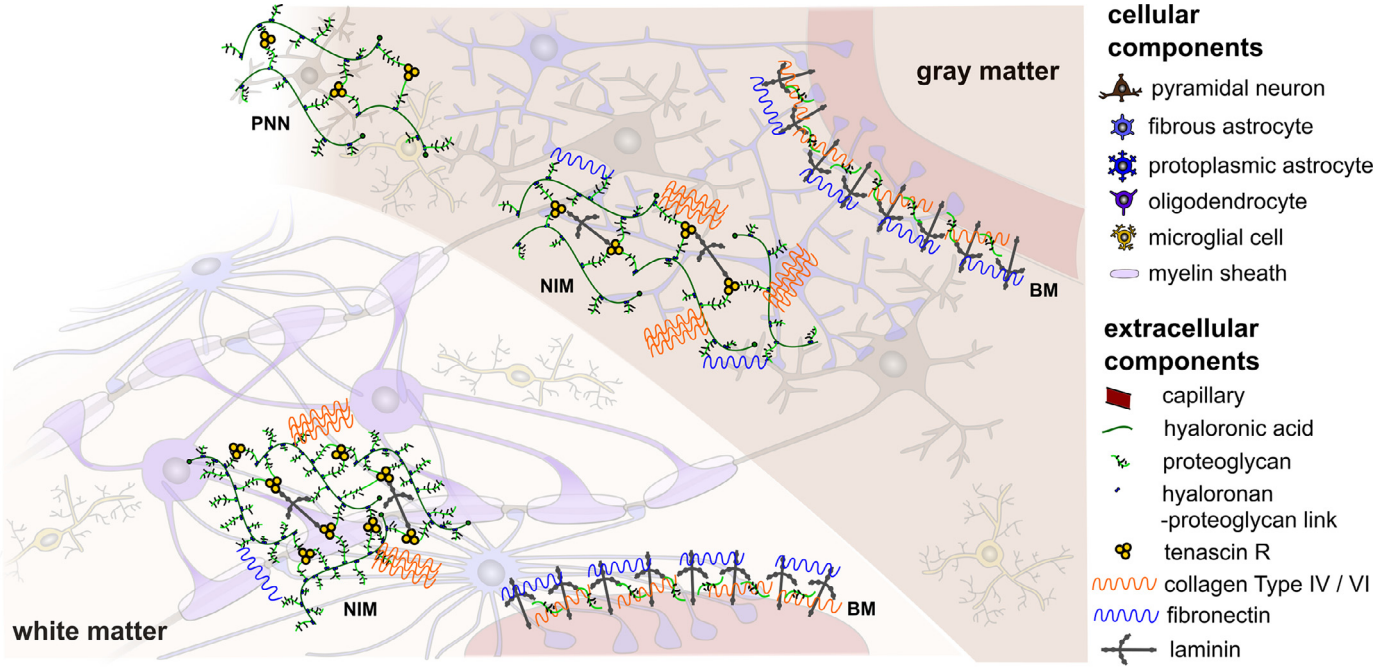

Fig. 7. Cellular and extracellular components of human brain tissue. White matter contains oligodendrocytes wrapping myelin sheath around axons, fibrous astrocytes, and microglia. Gray matter contains neurons, protoplasmic astrocytes, and microglia. The extracellular matrix has three principal compartments: the basement membrane (BM), which lines cerebral microvessels and the pial surface, the neural interstitial matrix (NIM), which is diffusely distributed in the brain's interstitial space, and perineuronal nets (PNN), which surround inhibitory interneurons in certain areas of gray matter. In different compositions, these compartments contain proteoglycans, hyaluronic acid, link proteins, glycoproteins (e.g., tenascin, laminin, fibronectin), and non-fibrillar collagens type IV and VI [7]. This is a schematic figure for identification purposes only with no claim of being complete or true to scale.

3.2.1. Cells

Fig. 8a shows that white matter regions contain more cell nuclei than gray matter regions (ANOVA: *F*-statistic=80.64, *p*-value=6.55e−29; for T–K pairwise comparisons see Table 1). Within white matter, more cells reside on average in the corona radiata than in the corpus callosum; within gray matter, more cells reside in the basal ganglia than in the cortex. However, the latter trends are not statistically significant. Notably, in this analysis we do not differentiate between different cell types: we equally treat neuronal cells and glial cells, including astrocytes, oligodendrocytes, microglial cells, and ependymal cells. While white matter tissue contains oligodendrocytes, which form myelin sheaths

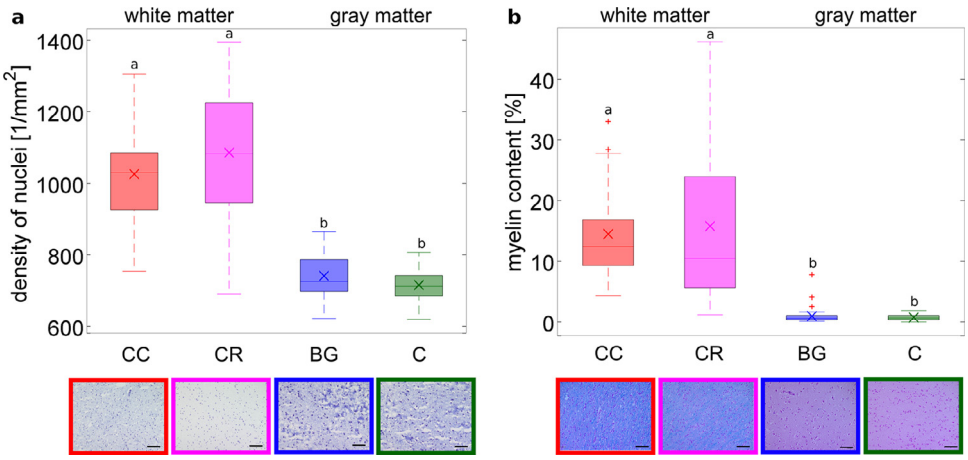

Fig. 8. Cellular components in different regions of the human brain, corpus callosum (CC), corona radiata (CR), basal ganglia (BG), and cortex (C). a) Density of cell nuclei quantified through Nissl staining. b) Myelin content quantified through Klüver–Barrera staining. Boxes indicate the median with 25th and 75th percentiles, the whiskers extend to the most extreme data points not considered outliers, while outliers are plotted individually using red plus symbols. In addition, the mean values are indicated by crosses. Statistically different groups are denoted by different letters (a and b). Scale bars in the stained images indicate 100 µm.

around nerve fibers, and fibrous astrocytes, which ensure supply of nutrients and synaptic processing, gray matter tissue contains neuronal cell bodies, the processing units of our brain, and protoplasmic astrocytes. Additionally, both white and gray matter contain microglial cells, which contribute to clearance of debris and synapse remodeling. More refined studies in the future could involve immunohistochemistry to investigate the distribution of individual cell types in different brain regions.

3.2.2. Myelin

Fig. 8b illustrates the area fraction of myelin, fatty sheath wrapped around nerve fibers to insulate signal propagation and improve electrical function. White matter specimens contained approximately 15% myelin, while gray matter specimens contained nearly 0% (ANOVA: F-statistic=30.06, p-value=8.63e−14; for T–K pairwise comparisons see Table 1). Within white matter, the amount of myelin was on average slightly higher in the corona radiata than in the corpus callosum.

3.2.3. Lipids

Fig. 9a shows that a higher lipid content was detected in the white matter than the gray matter (ANOVA: F-statistic=5.57, p-value=0.0036; for T–K pairwise comparisons see Table 1). This is not surprising since myelin, which is a lipid-rich layered material composed of phospholipid, cholesterol, and protein [30], is a major constituent of white matter tissue, as discussed in Section 3.2.2. Interestingly, however, individual lipid droplets appear larger in gray than in white matter, while white matter specimens have a higher overall intensity of red staining. Within white matter, the corona radiata has a slightly higher content of lipids than the corpus callosum; within gray matter, the cortex has a slightly higher lipid content than the basal ganglia.

Lipids occur in storage fat and as structural components in the cell membranes. It is generally known that roughly half of the mammalian brain's dry weight consists of lipids, which makes it the second most lipid-rich organ in the human body after adipose tissue.

3.2.4. Proteoglycans

Fig. 9b shows a clear difference between the proteoglycan content in gray and white matter (ANOVA: F-statistic=66.86, p-value=1.03e−31; for T–K pairwise comparisons see Table 1). White matter with an area fraction of about 20% contains significantly more proteoglycans than gray matter with only about 2%. The high variation even within the white matter specimens indicates that the proteoglycan distribution is quite heterogeneous, at least for the specimens tested in the current study – especially in the corpus callosum.

Proteoglycans are made up of a core protein to which glycosaminoglycan (GAG) side chains attach. Individual proteoglycans may differ in the composition of their core protein but also in the number and type of attached GAG chains [7]. Importantly, GAGs are negatively charged. Therefore, the proteoglycan content will most probably affect the water-binding properties and permeability of the tissue.

3.2.5. Collagen and cytoplasm

Fig. 9c demonstrates that regarding the collagen content, there is no clear difference between white and gray matter (ANOVA: F-statistic=13.15, p-value=5.24e−08; for T–K pairwise comparisons see Table 1). The results indicate that tissue from the corona radiata contains the least amount of collagen; tissue from the corpus callosum showed neither a significant difference to tissue from the basal ganglia nor from the cortex. Importantly, brain tissue contains mainly non-fibrillar collagen type IV, which differs from fibrillar collagen in the skin, arteries, or cartilage.

While we interpreted the amount of blue in Masson' Trichrome stained images as the collagen content (see Section 2.2.2), we interpret the amount of red as the cytoplasm content. Expectedly, Fig. 9d yields the opposite trends than Fig. 9c with highest content of cytoplasm in the corona radiata, and the lowest content in the basal ganglia (ANOVA: F-statistic=40.07, p-value=3.29e−21; for T–K pairwise comparisons see Table 1). Each of the brain regions showed significantly different amounts of cytoplasm. The findings agree well with the results in Section 3.2.1 as a higher density of cells will naturally lead to a higher amount of cytoplasm.

3.3. Correlation between microstructure and mechanics

To identify microstructural parameters that may be suitable for incorporation into microstructure-informed constitutive models for human brain tissue, we evaluate the correlations between microstructural components presented in Section 3.2 and mechanical properties in Section 3.1. Based on the results, appropriate model structures will be chosen in Section 3.4.

Fig. 10a suggests that the initial shear modulus μ negatively correlates with the density of cell nuclei: the more cells, the softer the tissue. One brain region, the basal ganglia, seems to stand out

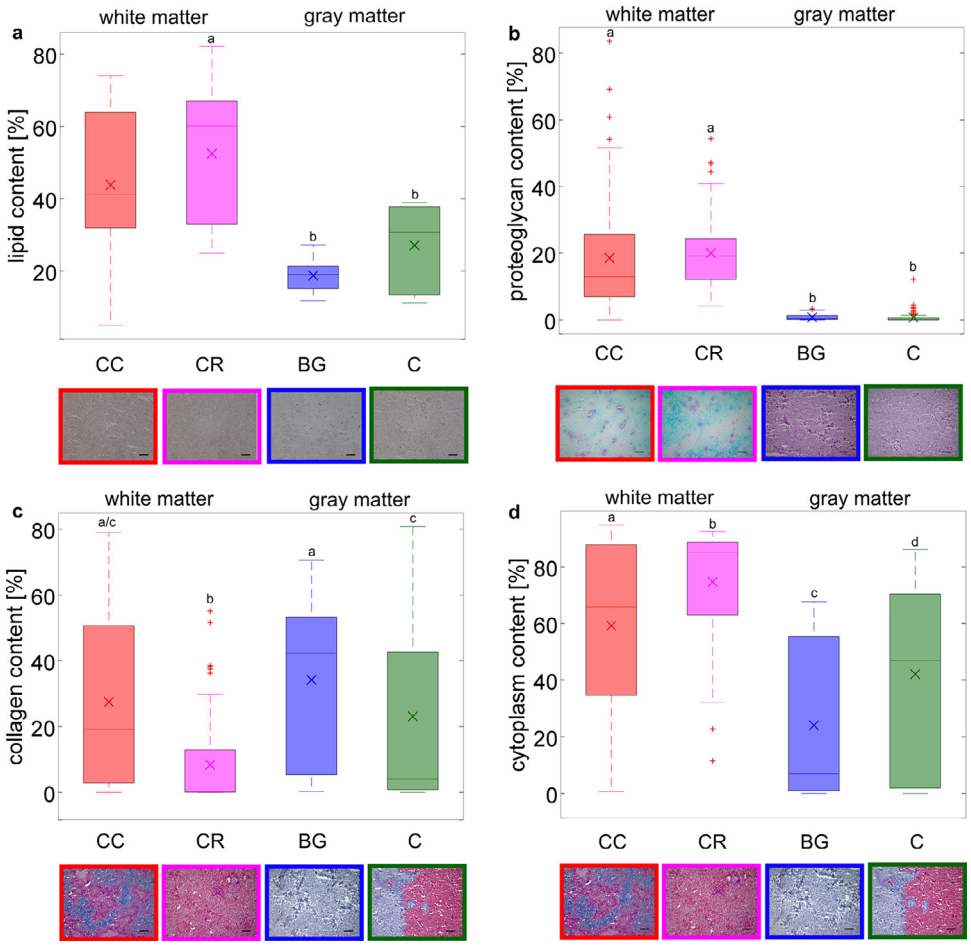

Fig. 9. Area fractions of extracellular matrix components in different regions of the human brain, corpus callosum (CC), corona radiata (CR), basal ganglia (BG), and cortex (C). a) Lipid content quantified through Oil Red staining. b) Proteoglycan content quantified through Alcian Blue staining. c) Collagen content quantified through Masson' Trichrome staining. d) Cytoplasm content quantified through Masson Trichome staining. Boxes indicate the median with 25th and 75th percentiles, the whiskers extend to the most extreme data points not considered outliers, while outliers are plotted individually using red plus symbols. In addition, the mean values are indicated by crosses. Statistically different groups are denoted by different letters (a, b, c, and d). Scale bars in the stained images indicate 100 µm.

with few cells per unit volume at relatively low stiffness. This could be attributed to the complex internal anatomical and neurochemical organization of this specific region; the structure significantly differs from that of surrounding tissue.

Fig. 10b shows that while the stiffness decreases with an increasing density of cell nuclei, the material nonlinearity – quantified by the absolute value of the nonlinearity parameter α – increases: the more cells, the higher the nonlinearity. Another characteristic which is associated with the nonlinearity parameter α is the compression-tension asymmetry. Therefore, our results indicate that more cells lead to an even higher difference between stresses in compression and in tension – the response under tensile loading is significantly softer than the response under compressive loading.

Fig. 10 c reveals a positive correlation between the myelin content and the tissue stiffness when comparing different white matter regions: the higher the myelin content, the higher the stiffness. Fig. 11a suggests that the nonlinearity of the brain tissue re-

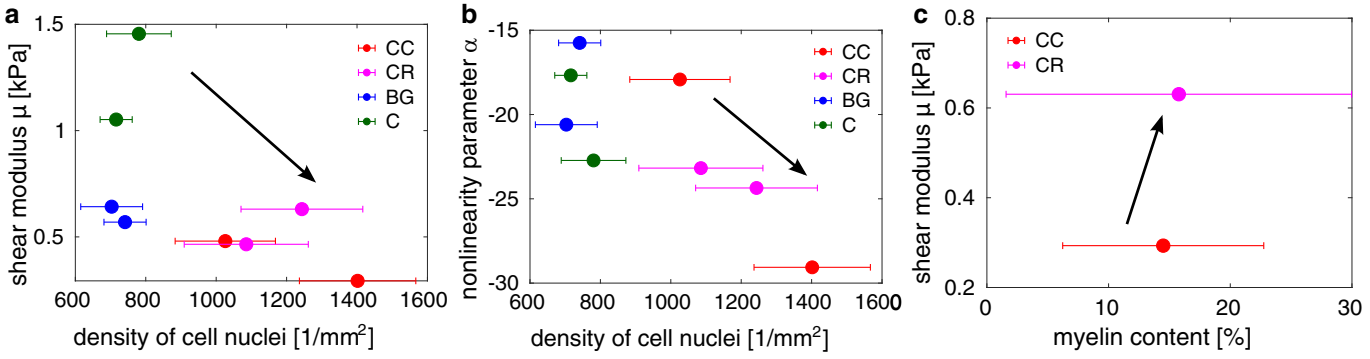

Fig. 10. Correlation between mechanics and cellular microstructural components (mean with standard deviations). a) Initial shear modulus μ versus density of cell nuclei. b) Nonlinearity parameter α versus density of cell nuclei. c) Initial shear modulus μ versus myelin content.

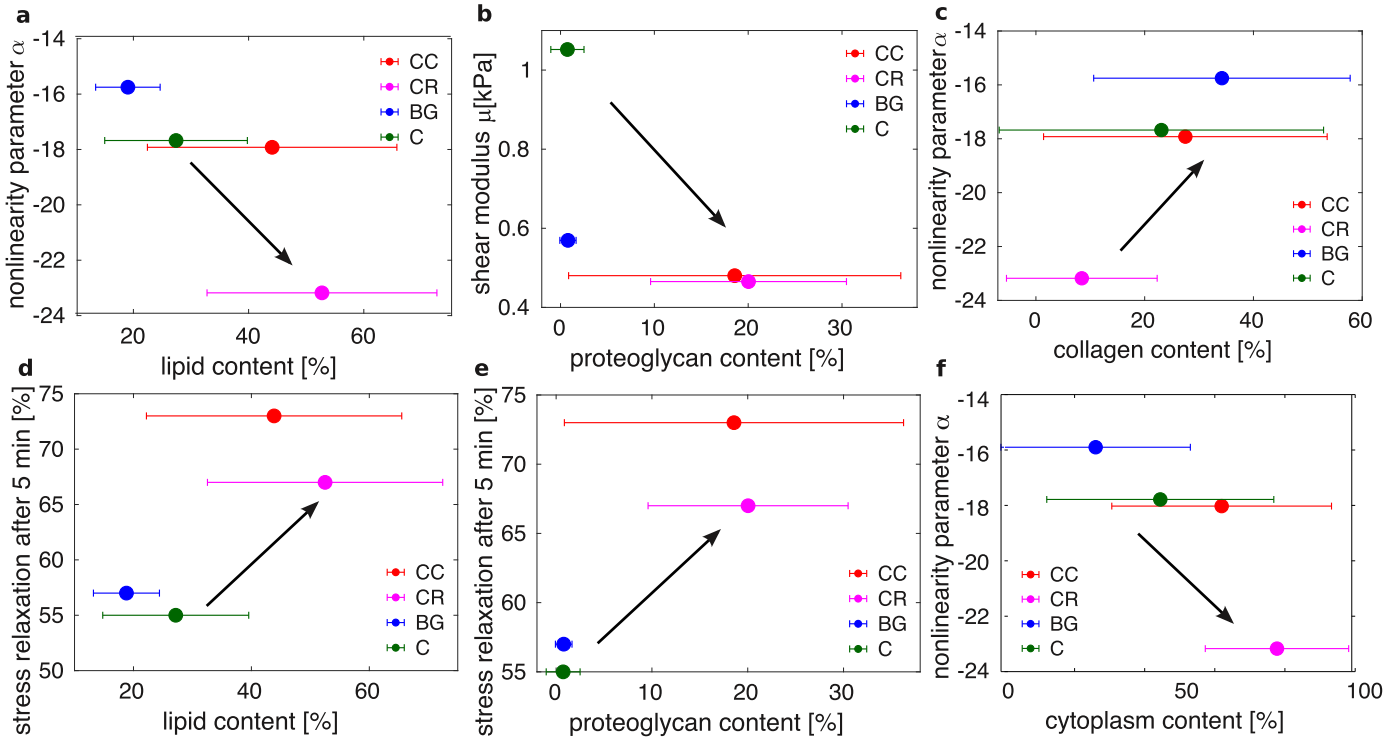

Fig. 11. Correlation between mechanics and extracellular matrix microstructural components (mean with standard deviations). a) Nonlinearity parameter α versus lipid content. b) Initial shear modulus μ versus proteoglycan content. c) Nonlinearity parameter α versus collagen content. d) Stress relaxation after 5 min versus lipid content. e) Stress relaxation after 5 min versus proteoglycan content. f) Nonlinearity parameter α versus cytoplasm content.

sponse increases with increasing lipid content: the higher the lipid content, the higher the material nonlinearity. In addition, the lipid content seems to positively correlate with the stress percentage relaxed after 5 min during relaxation experiments as shown in Fig. 11d: the higher the lipid content the faster the stress relaxation.

Fig. 11b indicates that the initial shear modulus of brain tissue decreases with increasing proteoglycan content: the more proteoglycans, the softer the tissue. Notably, similar to the results in Fig. 10a, one region, the basal ganglia, seems to stand out: both the proteoglycan content but also the stiffness are relatively low. Specimens with a higher proteoglycan content also generally showed higher stress relaxation after 5 min (see Fig. 11e): the more proteoglycans, the faster the stress relaxation.

Fig. 11c shows that the material nonlinearity and the compression-tension asymmetry – represented by the absolute value of the nonlinearity parameter α – decreases with increasing collagen content: the higher the collagen content, the lower the nonlinearity. As a natural consequence of this finding, Fig. 11f shows a positive correlation between the material nonlinearity and the cytoplasm content: the more cyctoplasm, the higher the nonlinearity.

3.4. Microstructure-informed material model

Inspired by the correlations in Fig. 10a and b, we propose to modify the one-term Ogden strain-energy introduced in Section 2.1, Eq. (1), by introducing the initial shear modulus μ and the nonlinearity parameter α as linear functions of the density of cell nuclei, which we denote by ρ_C, i.e.,

$$\psi(\rho_C) = 2\mu(\rho_C)/\alpha(\rho_C)^2[\lambda_1^{\alpha(\rho_C)} + \lambda_2^{\alpha(\rho_C)} + \lambda_3^{\alpha(\rho_C)} - 3], \tag{3}$$

with

$$\mu(\rho_C) = m_\mu\,\rho_C + c_\mu \quad \text{and} \quad \alpha(\rho_C) = m_\alpha\,\rho_C + c_\alpha. \tag{4}$$

Here, the correlations in Figs. 10 and 11 help us to choose the appropriate model framework. Importantly, to accurately calibrate the parameters m_μ, c_μ, m_α, and c_α, we use the raw experimental data in Fig. 5a and the mean cell densities for each region denoted by bold plus symbols in Fig. 8 as region-specific microstructural parameter ρ_C. We repeat the parameter calibration, as described in Section 3.1, but this time use the data from all regions simultaneously. Like this, we find a single set of parameters that is valid for all brain regions.

Fig. 12 shows the performance of the optimized microstructure-informed material model with $m_\mu = -0.0008$ kPa mm^2, $c_\mu = 1.3865$ kPa, $m_\alpha = -0.0037$ mm^2, and $c_\alpha = -14.3498$. The model is capable of simultaneously predicting the response of brain tissue under multiple loading modes, compression, tension, and simple shear, and for various brain regions, the corpus callosum, the corona radiata, the basal ganglia, and the cortex, fairly well. The model significantly deviates from the experimental response of the cortex specimen in simple shear, which can in part be attributed to the fact that, in general, this curve shows an exceptional behavior with an asymmetry between positive and negative amounts of shear. Apart from that, we observe the highest deviation for the basal ganglia specimen in compression and tension, which is in line with our previous observation that the qualitative response of basal ganglia tissue slightly differs from all other regions [11].

4. Discussion

Through the simultaneous analysis of microstructure and mechanics of human brain tissue from different anatomical regions, we have provided insights into the microstructural origin of the macroscopic mechanical tissue response. With respect to brain tissue mechanics, the current study not only evaluates the elasticity at small strains, but also considers nonlinear and time-dependent effects. With respect to brain tissue microstructure, we have not

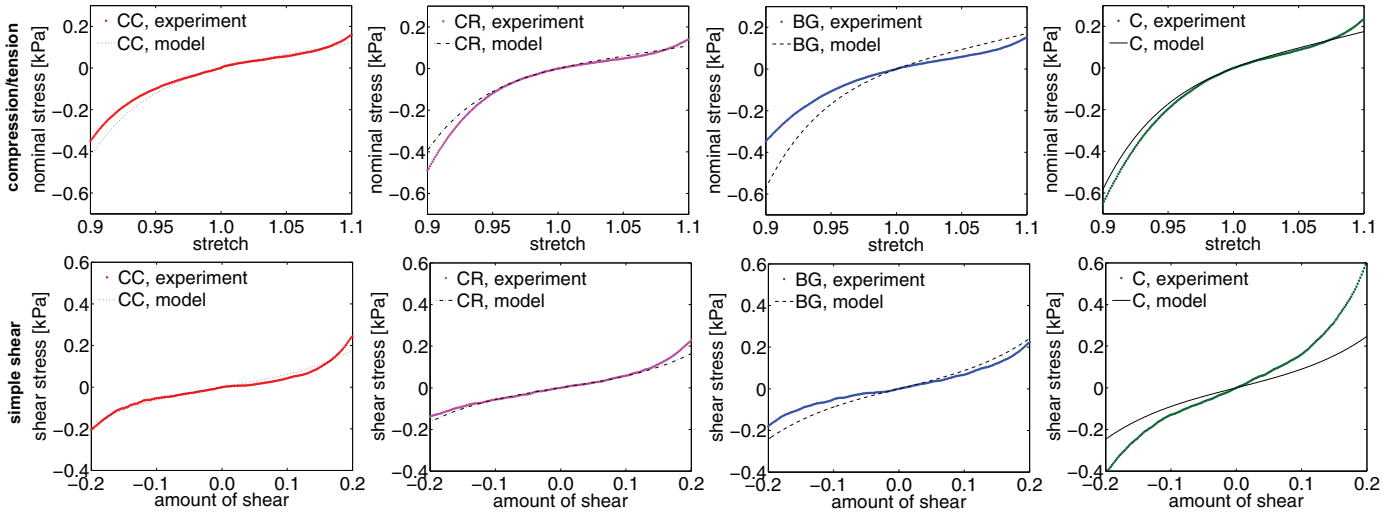

Fig. 12. Hyperelastic response of an exemplary specimen from four different brain regions, the cortex (C), the basal ganglia (BG), the corona radiata (CR), and the corpus callosum (CC) during compression, tension, and simple shear loadings fitted with a single microstructure-informed material model.

only examined cellular components – the functionally important elements of brain tissue – but have also considered extracellular matrix components.

4.1. Microstructural constituents in human brain tissue

According to our analyses, more cell nuclei are present in white matter than in gray matter. Notably, we did not distinguish between neuronal and glial cells in the current study. Therefore, in the future, more refined studies are necessary to additionally determine the distribution of individual cell types. In general, gray matter contains neurons and glial cells, while white matter contains mainly glial cells and neuronal axons, which doubtlessly results in considerable differences in the cellular network.

Interestingly, our results show that the distribution of extracellular matrix components is much more heterogeneous than the distribution of brain cells. In contrast, a previous study on rat spinal cord tissue had suggested that the extracellular matrix is comparatively homogeneously distributed [31]. This contradictory finding could either be attributed to differences between the brain parenchyma and the spinal cord, or to the fact that the central nervous system of humans is more complex and diverse than that of rodents. A systematic comparison of human brain and spinal cord tissue should be performed to answer this question in the future.

We have revealed a significant difference in the proteoglycan content between gray and white matter regions. While gray matter specimens hardly contain proteoglycans at all, white matter specimens contain an average area fraction of about 20% with significant local variations. The distribution of proteoglycans is highly relevant due to their important role for brain function. Proteoglycans affect the fixed charge density, the overall negative immobile charges of the tissue, and thereby directly influence the osmotic pressure, especially during brain swelling [1]. In addition, heparan sulfate proteoglycans control cell differentiation during neurogenesis [32,33], and another family of proteoglycans, chondroitin sulphate proteoglycans, seem to play an important role in myelin repair [7].

Similar to the distribution of proteoglycans, we found a clear difference between the lipid content in gray and white matter. Our results yield approximately 60% in white and 30% in gray matter, which is in agreement with previously reported data. For example, a study from 1968 reports that the lipid content in white matter (corona radiata) was 56% and in gray matter (cortex) 32%, similar to the results in Fig. 9a [34]. This confirms that the analysis of histological stains, as described in Section 2.2.2, yields reliable results. Lipids have been shown to play an important role during brain development, for instance concerning malformations such as microcephaly [35].

The distribution of collagen was even more heterogeneous than the distribution of proteoglycans and lipids. According to our results, the collagen content is highest in the corona radiata, lowest in the basal ganglia and comparable in the cortex and the corpus callosum.

Importantly, cellular and extracellular components of brain tissue cannot be regarded as independent. Astrocytes produce and secrete extracellular matrix constituents [36], therefore, an alteration in the density of astrocytes in the central nervous system will also lead to changes in the extracellular matrix and vice versa. Interestingly, the regulation of the extracellular matrix production by astrocytes appears to be sensitive to mechanical stimuli [37].

4.2. Insights into the microstructure-mechanics relation

We have found a negative correlation between the elastic tissue stiffness and the density of cell nuclei. This observation indicates that cells are the softest components of brain tissue, suggesting that they play an important role in terms of brain function but not necessarily in terms of brain mechanics. The results agree well with a recent study probing the elasticity of live mouse brain tissue on a much smaller scale by using atomic force microscopy, which also yielded a negative correlation between the relative cell nuclei area and the tissue stiffness [38]. In contrast to our findings, previous studies on brain tissue in the very early stages of development [39] or spinal cord tissue [40] showed a positive correlation between the relative tissue area covered by cell nuclei and the tissue stiffness. This emphasizes that brain tissue stiffness not only shows regional variations but may also change with age. In the early stages of brain development, when the dense network of intercellular connections, vasculature and extracellular matrix components has not yet formed, cells are actually the stiffest components and control the mechanical response. In this case, brain tissue stiffness shows a positive correlation with the density of nuclei [39]. We therefore conclude that the negative correlation between the density of cell nuclei and tissue stiffness is only valid for the fully developed brain and under physiological conditions. In cases where the interconnectivity of cells is disrupted, for instance due

to demyelination, this trend will not hold anymore [41]. Similarly, in patients suffering Alzheimer's disease, we would rather expect that the loss of neurons will lead to a decrease in tissue stiffness [42].

We have also found a positive correlation between the myelin content and the tissue stiffness. While two data points seem not enough to yield a clear trend, the observations confirm our previous nanoindentation experiments on bovine brain tissue of different developmental stages, which showed that brain tissue stiffness increases with the myelin content [14,15]. Notably, this trend is restricted to white matter specimens only, as gray matter tissue does not contain myelinated axons. The results indicate that myelin with the cellular coupling of axons via the glial matrix in large part dictates the mechanical response of the tissue [43].

Concerning the role of extracellular matrix components, we have found a negative correlation between the proteoglycan content and the tissue stiffness. This finding agrees well with observations in articular cartilage, where – during the process of aging – the content of proteoglycans decreases and the tissue becomes stiffer [44]. The loss of fixed charges associated with proteoglycan degradation limits the ability of cartilage to recover deformation [45]. Our results further indicate a correlation between the proteoglycan content and the stress relaxation behavior. This observation seems reasonable considering the fact that proteoglycans bind water molecules; the incompressible fluid trapped inside the tissue will initially contribute to the tissue's stiffness but slowly drain during the relaxation period due to the imposed load – leading to a decrease in the recorded stresses. The higher content of proteoglycans in white matter can therefore also explain why gray matter tissue (cortex and basal ganglia) exhibits a slightly smaller volume change compared to the white matter (corona radiata and corpus callosum) [46].

We further have found that the lipid content positively correlates with the material nonlinearity. This observation is in agreement with a recent study showing that high lipid contents in soft tissues lead to a highly nonlinear tissue response under large strains [47]. An important characteristic regarding combined loading conditions is that shear stresses increase significantly with superimposed compression, but only slightly with superimposed tension. This compression-tension asymmetry is again controlled by the nonlinearity parameter α: the higher the absolute value of α, the more pronounced the compression-tension asymmetry.

In contrast to lipids and proteoglycans, collagen seems to affect the elastic but not the viscous properties of brain tissue. Interestingly, our results indicate a negative correlation between the collagen content and the material nonlinearity. This finding seems counter-intuitive considering the fact that collagen has been identified as a stiffening component in other soft tissues such as arteries [48]. In this respect, it is important to note that brain tissue mostly contains non-fibrillar collagen, e.g., collagen type IV and VI, while fibrous tissues contain fibrillar collagen of types I and II. To the authors knowledge, the mechanics of non-fibrillar collagen remain largely unknown and need to be investigated in the future. According to our results, however, it engenders a softer, rather linear material response. This is also supported by the observation that the collagen IV content decreases during development [49], while the stiffness is known to increase [15]. In certain diseases such as multiple sclerosis, the level of fibrillar collagens increases. Those not only form a physical and chemical barrier for the recruitment of immune cells into the brain parenchyma [7], but will most likely also lead to an increase in tissue stiffness.

As cellular and extracellular constituents may change in tandem, it is difficult to specify their individual contributions to brain tissue mechanics. In the future, a systematic study covering a wide range of brain regions could refine the first insights we have presented in the current work. Understanding the correlation between brain mechanics and the underlying microstructure can also be highly valuable to identify biomarkers for neurological diseases or injury. Insults to the central nervous system, on the one hand, result in alterations to the brain's extracellular matrix, for instance, increased deposition of chondroitin sulphate proteoglycans and hyaluronan, wherein the extent depends on the severity and chronicity of the injury [7]. On the other hand, traumatic and degenerative conditions are often associated with loss of cellular components, for instance, loss of oligodendrocytes and demyelination [7].

4.3. Towards microstructure-based material models

A promising approach to overcome the issue that brain tissue properties highly vary in space and time is to introduce material models that are a function of microstructural components that show similar regional and temporal variations. When focusing on the time-independent, elastic response of brain tissue, the only component showing a positive correlation with the initial shear modulus was the myelin content. However, as this trend only applies to white matter regions, the myelin content is not the first choice for a microstructural parameter to be included into material models. But as the density of cell nuclei correlated with both the initial shear modulus and the nonlinearity parameter α, we have proposed to introduce these two parameters from the modified one-term Ogden model, Eq. (1), as a linear function of the density of cell nuclei ρ_C, as described in Section 3.4. The negative value of the parameter m_μ indicates that the mechanical response of brain tissue is largely controlled by the network of dendrites, synapses, and extracellular matrix, rather than the nuclei themselves. This notion is further supported by the observation that the trend between the density of nuclei and stiffness is reversed in the early stages of development [39], when the network of connections has not formed yet, as discussed in Section 4.2. Therefore, the microstructure-informed material model proposed in the current study is only valid for the fully developed brain under physiological conditions. Well-designed future combined mechanical and microstructural studies are needed to develop more advanced models that capture the response over a wider range of applications. The accuracy of model predictions could also be improved by distinguishing between the density of different cell types, by incorporating more than only one microstructural parameter, and by choosing higher order functions instead of the linear relations in Eq. (4).

We note that the lipid content showed a similar correlation with the nonlinearity parameter α as the density of cell nuclei, and the collagen content the reversed trend. However, as the density of nuclei can be more reliably determined using image processing techniques, it is better suited for the employment in microstructure-informed material models than the other quantities.

With regard to the time-dependent properties of brain tissue, both the proteoglycan content and the lipid content show positive correlations with the stress relaxed after 5 min. Therefore, those parameters are potential candidates for the incorporation into viscoelastic models for brain tissue behavior, e.g. by introducing the viscosity as a function of one of these microstructural parameters.

4.4. Limitations

The human brains studied here originate from elderly subjects [11] and could therefore be affected by age-related changes in the tissue's microstructure. Additional experiments need to be performed in the future to confirm and refine the observed trends, also with regard to the small sample size in the current study. Still, we would like to emphasize that it is extremely difficult to obtain

and mechanically test human tissue samples, both from a practical but also from an ethical point of view. We therefore strongly believe that despite rather few data points, the current study is highly valuable to drive the future directions of material models for human brain tissue and to more carefully plan future experiments.

An additional limitation arises from the fact that we tested brain tissue *ex vivo*. To date, the question how *ex vivo* brain tissue properties compare to the *in vivo* response remains ambiguous. Indentation experiments on rat brains, ultrasound elastography measurements, and a magnetic resonance elastography study on porcine brain tissue yielded 30–50% higher moduli *in vivo* than *ex vivo* [21,22,49–51], while other studies using magnetic resonance elastography showed only small differences [52], or even the opposite trend [53]. As *in vivo* magnetic resonance elastography is limited to small deformations and highly depends on the method used to extract elastic properties, as well as the excitation frequencies, this technique is insufficient to fully characterize the highly nonlinear tissue response at large strains [54].

We have further noticed that the absolute area fractions of tissue components showed a slight sensitivity towards the magnification of the images, which was used for analysis; the regional trends, in contrast, were highly consistent. This emphasizes that when including microstructural information in material models for brain tissue, it is important to use the exact same analysis method for calibration and application.

5. Conclusion

In the current study, we have simultaneously analyzed the microstructural composition and nonlinear mechanical properties of human brain tissue. We have provided insights into regional differences in the distribution of cell nuclei, myelin, lipids, proteoglycans, and collagen, and their correlation with the complex mechanical properties of human brain tissue. Our study reveals a negative correlation between the cell count and the stiffness, a positive correlation between myelin content and stiffness, and a negative correlation between proteoglycan content and the stiffness. It further indicates a positive correlation between lipid and proteoglycan content and viscosity. Understanding the microstructural origin of macroscopic brain tissue mechanics will help us design more precise, multi-scale models for computational simulations of human brain tissue behavior. This is a critical step towards a better understanding of the role of mechanics for clinical conditions including cortical malformations, chronic traumatic encephalopathy, Alzheimer's and Parkinson's disease, or multiple sclerosis

Author Contributions

GAH, PS, GS, EK, and SB designed the study. GH, GS, and SB supervised the mechanical testing and modeling. SB performed the mechanical modeling and analysis. FP and NP performed the staining for cellular components and imaging. MS and LS performed the staining for extracellular components. VPS supervised the analysis of extracellular components and brought up the role of proteoglycans. JP and SB analyzed the data. SB wrote the original draft. All authors have discussed the results and reviewed the final manuscript.

Declaration of Competing Interest

The authors declare that they have no known competing financial interests or personal relationships that could have appeared to influence the work reported in this paper.

Acknowledgements

The financial support by the German Research Foundation grants STE 544/50 and BU 3728/1-1 to PS and SB, as well as the Emerging Talents Initiative to SB and the Emerging Fields Initiative by the FAU to PS, SB, and FP is gratefully acknolwedged. We further acknowledge funding by the National Science Foundation grant CMMI 1727268 as well as the Stanford Bio-X IIP seed grant and the Humboldt Research Award to EK. VPS acknowledges DFG funding via the Federal and State government excellence inititaive (EXC 294).

References

[1] A. Goriely, M.G. Geers, G.A. Holzapfel, J. Jayamohan, A. Jérusalem, S. Sivaloganathan, W. Squier, J.A. van Dommelen, S. Waters, E. Kuhl, Mechanics of the brain: perspectives, challenges, and opportunities, Biomech. Model. Mechanobiol. 14 (5) (2015) 931–965.
[2] J.M. Barnes, L. Przybyla, V.M. Weaver, Tissue mechanics regulate brain development, homeostasis and disease, J. Cell. Sci. 130 (1) (2017) 71–82.
[3] D.F. Meaney, B. Morrison, C.D. Bass, The mechanics of traumatic brain injury: a review of what we know and what we need to know for reducing its societal burden, J. Biomech. Eng. 136 (2) (2014) 021008.
[4] Y. Feng, Y. Gao, T. Wang, L. Tao, S. Qiu, X. Zhao, A longitudinal study of the mechanical properties of injured brain tissue in a mouse model, J. Mech. Behav. Biomed. Mater. 71 (2017) 407–415.
[5] W.J. Tyler, The mechanobiology of brain function, Nat. Rev. Neurosci. 13 (12) (2012) 867–878.
[6] D.E. Koser, A.J. Thompson, S.K. Foster, A. Dwivedy, E.K. Pillai, G.K. Sheridan, H. Svoboda, M. Viana, L. da F Costa, J. Guck, et al., Mechanosensing is critical for axon growth in the developing brain, Nat. Neurosci. 19 (12) (2016) 1592–1598.
[7] L.W. Lau, R. Cua, M.B. Keough, S. Haylock-Jacobs, V.W. Yong, Pathophysiology of the brain extracellular matrix: a new target for remyelination, Nat. Rev. Neurosci. 14 (10) (2013) 722–729.
[8] N.R. Blumenthal, O. Hermanson, B. Heimrich, V.P. Shastri, Stochastic nanoroughness modulates neuron–astrocyte interactions and function via mechanosensing cation channels, Proc. Natl. Acad. Sci. USA 111 (45) (2014) 16124–16129.
[9] M.T. Begonia, R. Prabhu, J. Liao, M.F. Horstemeyer, L.N. Williams, The influence of strain rate dependency on the structure–property relations of porcine brain, Ann. Biomed. Eng. 38 (10) (2010) 3043–3057.
[10] J. Weickenmeier, C. Butler, P. Young, A. Goriely, E. Kuhl, The mechanics of decompressive craniectomy: personalized simulations, Comp. Methods Appl. Mech. Eng. 314 (2017) 180–195.
[11] S. Budday, G. Sommer, C. Birkl, C. Langkammer, J. Haybaeck, J. Kohnert, M. Bauer, F. Paulsen, P. Steinmann, E. Kuhl, G.A. Holzapfel, Mechanical characterization of human brain tissue, Acta Biomater. 48 (2017) 319–340, doi:10.1016/j.actbio.2016.10.036.
[12] G.A. Holzapfel, Nonlinear Solid Mechanics: A Continuum Approach for Engineering Science, 24, John Wiley & Sons, Chichester, 2000.
[13] Y.-B. Lu, K. Franze, G. Seifert, C. Steinhäuser, F. Kirchhoff, H. Wolburg, J. Guck, P. Janmey, E.-Q. Wei, J. Käs, et al., Viscoelastic properties of individual glial cells and neurons in the CNS, Proc. Natl. Acad. Sci. USA 103 (47) (2006) 17759–17764.
[14] J. Weickenmeier, R. de Rooij, S. Budday, P. Steinmann, T.C. Ovaert, E. Kuhl, Brain stiffness increases with myelin content, Acta Biomater. 42 (2016) 265–272.
[15] J. Weickenmeier, R. de Rooij, S. Budday, T.C. Ovaert, E. Kuhl, The mechanical importance of myelination in the central nervous system, J. Mech. Behav. Biomed. Mater. 76 (2017) 119–124.
[16] S. Budday, G. Sommer, J. Haybaeck, P. Steinmann, G.A. Holzapfel, E. Kuhl, Rheological characterization of human brain tissue, Acta Biomater. 60 (2017) 315–329, doi:10.1016/j.actbio.2017.06.024.
[17] S. Budday, G. Sommer, P. Steinmann, G.A. Holzapfel, E. Kuhl, Viscoelastic parameter identification of human brain tissue, J. Mech. Behav. Biomed. Mater. 74 (2017) 463–476, doi:10.1016/j.jmbbm.2017.07.014.
[18] G. Sommer, M. Eder, L. Kovacs, H. Pathak, L. Bonitz, C. Mueller, P. Regitnig, G.A. Holzapfel, Multiaxial mechanical properties and constitutive modeling of human adipose tissue: a basis for preoperative simulations in plastic and reconstructive surgery, Acta Biomater. 9 (11) (2013) 9036–9048.
[19] R.W. Ogden, Large deformation isotropic elasticity-on the correlation of theory and experiment for incompressible rubberlike solids, Proc. R. Soc. A 326 (1567) (1972) 565–584.
[20] S. Budday, R. Nay, R. de Rooij, P. Steinmann, T. Wyrobek, T.C. Ovaert, E. Kuhl, Mechanical properties of gray and white matter brain tissue by indentation, J. Mech. Behav. Biomed. Mater. 46 (2015) 318–330, doi:10.1016/j.jmbbm.2015.02.024.
[21] K. Miller, Constitutive model of brain tissue suitable for finite element analysis of surgical procedures, J. Biomech. 32 (5) (1999) 531–537.
[22] A. Gefen, S.S. Margulies, Are in vivo and in situ brain tissues mechanically similar? J. Biomech. 37 (2004) 1339–1352.

[23] M.T. Prange, S.S. Margulies, Regional, directional, and age-dependent properties of the brain undergoing large deformation, J. Biomech. Eng. 124 (2) (2002) 244–252.
[24] M. Sarem, N. Arya, M. Heizmann, A.T. Neffe, A. Barbero, T.P. Gebauer, I. Martin, A. Lendlein, V.P. Shastri, Interplay between stiffness and degradation of architectured gelatin hydrogels leads to differential modulation of chondrogenesis in vitro and in vivo, Acta Biomater. 69 (2018) 83–94.
[25] M. Sarem, M. Heizmann, A. Barbero, I. Martin, V.P. Shastri, Hyperstimulation of CaSR in human MSCs by biomimetic apatite inhibits endochondral ossification via temporal down-regulation of PTH1R, Proc. Natl. Acad. Sci. USA 115 (27) (2018) E6135–E6144.
[26] M. Sarem, O. Otto, S. Tanaka, V.P. Shastri, Cell number in mesenchymal stem cell aggregates dictates cell stiffness and chondrogenesis, Stem Cell Res. Ther. 10 (1) (2019) 10.
[27] M. Lukashevich, V. Starovoitov, An approach to cell nuclei counting in histological image analysis, in: IFIP International Conference on Computer Information Systems and Industrial Management, Springer, 2016, pp. 139–147.
[28] K. Miller, K. Chinzei, Mechanical properties of brain tissue in tension, J. Biomech. 35 (4) (2002) 483–490.
[29] Y. Lei, H. Han, F. Yuan, A. Javeed, Y. Zhao, The brain interstitial system: anatomy, modeling, in vivo measurement, and applications, Prog. Neurobiol. 157 (2017) 230–246.
[30] S. Schmitt, L.C. Castelvetri, M. Simons, Metabolism and functions of lipids in myelin, Biochim. Biophys. Acta, Mol. Cell. Biol. Lipids 1851 (8) (2015) 999–1005.
[31] C.M. Galtrey, J.C. Kwok, D. Carulli, K.E. Rhodes, J.W. Fawcett, Distribution and synthesis of extracellular matrix proteoglycans, hyaluronan, link proteins and tenascin-r in the rat spinal cord, Eur. J. Neurosci. 27 (6) (2008) 1373–1390.
[32] C.M. Galtrey, J.W. Fawcett, The role of chondroitin sulfate proteoglycans in regeneration and plasticity in the central nervous system, Brain Res. Rev. 54 (1) (2007) 1–18.
[33] W.-L. Gu, S.-L. Fu, Y.-X. Wang, Y. Li, H.-Z. Lü, X.-M. Xu, P.-H. Lu, Chondroitin sulfate proteoglycans regulate the growth, differentiation and migration of multipotent neural precursor cells through the integrin signaling pathway, BMC Neurosci. 10 (1) (2009) 128.
[34] A.K. Ommaya, Mechanical properties of tissues of the nervous system, J. Biomech. 1 (2) (1968) 127–138.
[35] C. Betsholtz, Lipid transport and human brain development, Nat. Genet. 47 (7) (2015) 699–701.
[36] R.J. McKeon, R.C. Schreiber, J.S. Rudge, J. Silver, Reduction of neurite outgrowth in a model of glial scarring following CNS injury is correlated with the expression of inhibitory molecules on reactive astrocytes, J. Neurosci. 11 (11) (1991) 3398–3411.
[37] A. Walker, J. Kim, J. Wyatt, A. Terlouw, K. Balachandran, J. Wolchok, Repeated in vitro impact conditioning of astrocytes decreases the expression and accumulation of extracellular matrix, Ann. Biomed. Eng. 47 (4) (2019) 967–979.
[38] N. Antonovaite, S.V. Beekmans, E.M. Hol, W.J. Wadman, D. Iannuzzi, Regional variations in stiffness in live mouse brain tissue determined by depth-controlled indentation mapping, Sci. Rep. 8 (1) (2018) 12517.
[39] A.J. Thompson, E.K. Pillai, I.B. Dimov, S.K. Foster, C.E. Holt, K. Franze, Rapid changes in tissue mechanics regulate cell behaviour in the developing embryonic brain, eLife 8 (2019) e39356.
[40] D.E. Koser, E. Moeendarbary, J. Hanne, S. Kuerten, K. Franze, CNS cell distribution and axon orientation determine local spinal cord mechanical properties, Biophys. J. 108 (9) (2015) 2137–2147.
[41] C. Lucchinetti, W. Brück, J. Parisi, B. Scheithauer, M. Rodriguez, H. Lassmann, Heterogeneity of multiple sclerosis lesions: implications for the pathogenesis of demyelination, Ann. Neurol. 47 (6) (2000) 707–717.
[42] M.C. Murphy, D.T. Jones, C.R. Jack Jr, K.J. Glaser, M.L. Senjem, A. Manduca, J.P. Felmlee, R.E. Carter, R.L. Ehman, J. Huston III, Regional brain stiffness changes across the Alzheimer's disease spectrum, NeuroImage 10 (2016) 283–290.
[43] D.I. Shreiber, H. Hao, R.A. Elias, Probing the influence of myelin and glia on the tensile properties of the spinal cord, Biomech. Model. Mechanobiol. 8 (4) (2009) 311–321.
[44] M. Lotz, R.F. Loeser, Effects of aging on articular cartilage homeostasis, Bone 51 (2) (2012) 241–248.
[45] L.J. Bonassar, E.H. Frank, J.C. Murray, C.G. Paguio, V.L. Moore, M.W. Lark, J.D. Sandy, J.-J. Wu, D.R. Eyre, A.J. Grodzinsky, Changes in cartilage composition and physical properties due to stromelysin degradation, Arthritis Rheum. 38 (2) (1995) 173–183.
[46] G.Z. Voyiadjis, A. Samadi-Dooki, Hyperelastic modeling of the human brain tissue: effects of no-slip boundary condition and compressibility on the uniaxial deformation, J. Mech. Behav. Biomed. Mater. 83 (2018) 63–78.
[47] L.A. Mihai, A. Goriely, How to characterize a nonlinear elastic material? a review on nonlinear constitutive parameters in isotropic finite elasticity, Proc. R. Soc. A 473 (2207) (2017) 20170607.
[48] G.A. Holzapfel, R.W. Ogden, Constitutive modelling of arteries, Proc. R. Soc. A 466 (2010) 1551–1597.
[49] A.V. Shulyakov, S.S. Cenkowski, R.J. Buist, M.R. Del Bigio, Age-dependence of intracranial viscoelastic properties in living rats, J. Mech. Behav. Biomed. Mater. 4 (3) (2011) 484–497.
[50] Y.-L. Liu, D. Liu, L. Xu, C. Su, G.-Y. Li, L.-X. Qian, Y. Cao, In vivo and ex vivo elastic properties of brain tissues measured with ultrasound elastography, J. Mech. Behav. Biomed. Mater. 83 (2018) 120–125.
[51] C.A. Guertler, R.J. Okamoto, J.L. Schmidt, A.A. Badachhape, C.L. Johnson, P.V. Bayly, Mechanical properties of porcine brain tissue in vivo and ex vivo estimated by mr elastography, J. Biomech. 69 (2018) 10–18.
[52] J. Vappou, E. Breton, P. Choquet, R. Willinger, A. Constantinesco, Assessment of in vivo and post-mortem mechanical behavior of brain tissue using magnetic resonance elastography, J. Biomech. 41 (14) (2008) 2954–2959.
[53] J. Weickenmeier, M. Kurt, E. Ozkaya, R. de Rooij, T.C. Ovaert, R. Ehman, K.B. Pauly, E. Kuhl, Brain stiffens post mortem, J. Mech. Behav. Biomed. Mater. 84 (2018) 88–98.
[54] S. Papazoglou, S. Hirsch, J. Braun, I. Sack, Multifrequency inversion in magnetic resonance elastography, Phys. Med. Biol. 57 (8) (2012) 2329.